Geophys. J. Int. (2005) **160,** 761–775 doi: 10.1111/j.1365-246X.2005.02519.x

The dynamics of subduction and trench migration for viscosity stratification

Alwina Enns,[1] Thorsten W. Becker[2★] and Harro Schmeling[1]

[1]*Institute of Meteorology and Geophysics, J. W. Goethe University, Feldbergstr.* 47, 60323 *Frankfurt am Main, Germany.*
E-mail: enns@geophysik.uni-frankfurt.de
[2]*Cecil H. and Ida M. Green Institute of Geophysics and Planetary Physics, Scripps Institution of Oceanography, University of California, San Diego,* 9500 *Gilman Drive, La Jolla* CA 92093, *USA*

Accepted 2004 October 29. Received 2004 October 21; in original form 2003 December 12

SUMMARY

Although subduction plays a dominant role in plate tectonics, related processes such as trench migration are not well understood. We investigate the influence of viscosity stratification and different flow boundary conditions on the trench migration dynamics of a subducting lithosphere in a 2-D model using a finite-difference code. Subduction and mantle flow are driven by a compositionally prescribed density contrast between the high-viscosity slab and the ambient mantle; no overriding plate is assumed. The model rheology is viscoplastic at shallow, and viscous at greater depth; the mantle is stratified with a higher viscosity in the lower part of the computational domain. The plastic rheology allows the plate to decouple from the top of the box and is described by a simplified friction law to mimic the brittle deformation of the shallow lithosphere. The flow patterns and slab morphologies differ as a function of the velocity boundary conditions (BCs). For reflective BCs, we model either a plate which is fixed on the box side or a plate that can freely move. A slab with periodic BCs is always laterally free. We find that, when the slabs interact with the highly viscous lower mantle, the slab with reflective BCs is more folded than the periodic one, due to the confinement of mantle flow around the slab. In general, the trench is observed to roll back toward the oceanic plate. For free slabs with reflective BCs the trench retreat velocity deceases after the interaction with the lower mantle. In contrast, for the free slab with periodic BCs it is nearly constant or even increases with time if described in a reference frame fixed to the lower mantle. The free slab with periodic BCs exerts a force on the lower mantle, which causes a net differential flow between the upper and lower mantle. We also carried out additional experiments with different mechanical slab properties and thicknesses. Stiffer, free slabs subduct more steeply and are able to penetrate straight into the lower mantle. After penetration into the lower mantle the trench moves toward the continent. Thinner slabs deform more easily and are folded for all boundary conditions. We can generalize the rollback systematics for free slabs by normalizing trench velocities by the plate speed. Free slabs, being more representative of the West Pacific subduction zones, show large temporal variations of normalized trench velocities ranging between a retreat value of 1.0 to an advancing value of −0.3.

Key words: flow boundary conditions, slab rollback, subduction, viscosity stratification.

1 INTRODUCTION

From first principles of plate tectonics it follows that subduction zones and trenches are not stationary features but that they migrate with respect to an absolute reference frame such as the hotspot reference frame (e.g. Garfunkel *et al.* 1986). In fact, the opening of oceans surrounded by passive margins requires a net closure of oceans bounded by subduction zones being associated with a net trench rollback. Until the early 1990s trench migration velocities were inferred from evaluation of the kinematics of global plate motions. Using simplified assumptions such as vertical downwelling at subduction zones, the horizontal migration of trenches at subduction zones was related to the dip angle of subduction. The problem with these early models was that many subduction zones are not fixed at continental plate margins, but instead are separated from these by backarc basins. Due to uncertainties in the extension rates

★Now at: Department of Earth Sciences, University of Southern California, Los Angeles, CA 90089-0740, USA.

of these backarc basins trench migration rates have been uncertain. In the last years this situation has changed dramatically due to direct GPS measurements. For example, Bevis *et al.* (1995) observed very fast extension of the Lau Basin (backarc basin of the Tonga subduction zone), implying trench migration velocities of up to 16 cm yr^{-1}. GPS campaigns in other Pacific subduction regions now allow one to quantify the rollback effect and backarc spreading directly. Kato *et al.* (1998) inferred trench migration velocities of 4.4 and 5 cm yr^{-1} for the Ryukyu and Mariana subduction zones, respectively. From GPS measurements in the Andean region (Sella *et al.* 2002) one can estimate trench migration velocities of the Andean Trench of the order of 1 cm yr^{-1}. Another region of pronounced trench rollback is the Mediterranean: tectonic reconstructions and GPS measurements suggest trench rollback of the Calabria Trench during the last 38 Myr with a peak rate of 12 cm yr^{-1} and a recent migration velocity of 5 to 6 cm yr^{-1} (geological indicators) or about 0 cm yr^{-1} (GPS), and of the Hellenic Trench during the last 18 Myr with a rate of 3 to 5 cm yr^{-1} (Heidbach 1999; McClusky *et al.* 2000; Faccenna *et al.* 2003b).

The causes and the physics of trench motion are not well understood. Attempts at geodynamic modelling can be divided into two categories: (1) those which prescribe the trench migration kinematics and (2) those with dynamically free trench migration (but sometimes with kinematically prescribed plate velocities).

1.1 Prescribed trench migration models

The first set of models has been used to investigate the relation between trench migration, slab deformation and slab penetration into the lower mantle. Christensen (1996) introduced an elegant concept of modelling subduction of a cold and highly viscous slab into a viscous mantle by prescribing a high-temperature surface boundary condition on the overriding side of the subduction zone. This method effectively decouples the subducting slab from the overriding region, and guarantees contiguity of the slab within the shallow subduction zone. A different approach was used by Olbertz *et al.* (1997), who assumed a smooth kinematic transition between subducting slab and overriding lithosphere. In the laboratory models of Griffiths *et al.* (1995), the subduction process was induced by feeding a highly viscous 'slab fluid' directly into the laterally moving 'mantle fluid'. From all these approaches it turned out that the resulting dip angle in the upper mantle strongly depends on the prescribed trench migration velocity, that higher migration velocities lead to slab flattening near the 660 km discontinuity (as observed in seismic tomography for some cases) and that slab penetration into the highly viscous lower mantle is delayed for fast trench migration velocities. The question arises whether in nature these effects are causes or consequences of trench migration.

1.2 Free trench migration models

In the majority of the laboratory and numerical models of Becker *et al.* (1999a) convergence velocities of the subducting and overriding plates were kinematically prescribed, while the trench evolved dynamically in a self-consistent way. Becker *et al.* observed that trench migration may be oceanward or continentward depending on the buoyancy contrast between the slab and the mantle. With these models questions arise about how strongly the results are influenced by the prescribed kinematic side boundary conditions which control the horizontal forces in the slab. In a more self-consistent way Zhong & Gurnis (1995a,b), Han & Gurnis (1999) and Gurnis *et al.* (2000) have modelled subduction as part of a large-scale mantle convection flow, using a special fault formulation to dynamically decouple the subducting slab from the overriding plate. They obtained a fast trench rollback effect during the early stages of subduction as long as the slab encounters the high resistance of the 660 km phase boundary and the highly viscous lower mantle. Upon penetrating into the lower mantle, trench migration slows down. These authors used large models with free oceanic plates with a length of 10 000 km. Whether their results may be applicable to smaller plates and/or plates with old continents (such as the Mediterranean cases) remains to be investigated.

Free trench migration has also been observed in the subduction models of Tetzlaff & Schmeling (2000). They modelled self-consistent subduction of a non-Newtonian slab utilizing the 'hot overriding mantle method' (Christensen 1996, see above) and focused on the kinetics of the olivine, spinel and perovskite phase transitions. Due to the increased resistance at the 660 km discontinuity trench rollback has been observed, which depends linearly on the age of the subducting slab. Furthermore, a slight increase in migration velocity occurs due to the presence of metastable olivine for old slabs. The modelled migration velocities agree well with the classical values determined by Garfunkel *et al.* (1986). However, the observed migration velocities of the Tonga and the Calabria trenches seem to be significantly higher, suggesting that other mechanisms may be responsible. The question arises of how much the trench migration is influenced by the symmetric side boundary conditions of these models.

Funiciello *et al.* (2003b) carried out numerical models of retreating slabs with visco-elastoplastic rheology predicting dip angles and retreat velocities. However, mantle forces which act on the downgoing slab were mimicked by dashpots, neglecting viscous stresses and dynamic pressures. A thorough series of 3-D laboratory experiments on retreating slabs was carried out by Funiciello *et al.* (2003a). They identify several stages of subduction, most importantly the free-fall stage of the slab sinking through the upper mantle, and a later steady state as the slab sinks into the lower mantle. During the free-fall stage, the retreat velocity increases exponentially until it becomes constant after interaction of the slab with the lower mantle. Interestingly, Funiciello (2002) point out the importance of laterally free versus closed boundary conditions (at the sides perpendicular to the trench), allowing for 3-D flow of mantle material around the slab. This significantly increases the magnitude of the retreat velocity. As their slabs are fixed to the non-subducting side of the model, any subduction of the (non-stretching) slab has to result in trench retreat for geometric reasons. Thus, the modelled trench migration velocities are identical to the relative velocity of the slab approaching the subduction zone. It thus remains to be investigated how non-fixed slabs behave and whether trench migration velocities are smaller.

In the following we present a series of 2-D numerical models of subduction focusing on the trench retreat as the slab sinks through the upper mantle and subsequently interacts with the highly viscous lower mantle. We first address the question of the decoupling mechanism from the overriding medium at the trench. We then focus on the importance of different boundary conditions and compare cases with symmetric (i.e. closed) and periodic (i.e. open) boundary conditions as well as laterally free versus fixed slabs. Then the effect of slab properties on the retreat velocity will be addressed. One of our major findings, a net differential velocity between the upper and lower mantle (e.g. Davies 1999), leads to the question of the appropriate choice of reference frame. We also find that slab folding within the lower mantle strongly depends on the degree of flow constraints and slab properties.

2 MODEL AND METHOD

Our goal is to understand the dynamics of slab rollback and the interaction of the subducting lithosphere with mantle currents in a mantle with stratified viscosity. To isolate these effects, we model only the sinking oceanic plate and not the overriding plate (Christensen 1996). Under the Boussinesq approximation, mantle convection in the infinite Prandtl number limit can be described by the continuity equation:

$$\nabla \cdot \mathbf{v} = 0 \tag{1}$$

with velocity, **v**, and the conservation of momentum equation

$$-\nabla p + \nabla \cdot \tau + \Delta\rho \mathbf{g} = 0. \tag{2}$$

Here, τ, p and **g** denote the deviatoric stress tensor, dynamic pressure and gravitational acceleration, respectively. We will neglect thermal effects and not solve the energy equation but assign a single density contrast, $\Delta\rho|_{\mathrm{slab}}$, between the slab and the surrounding mantle. We choose a viscoplastic rheology for the whole model domain such that

$$\tau = 2\eta_{\mathrm{eff}}\dot{\epsilon} \tag{3}$$

where $\dot{\epsilon}$ is the strain rate tensor. The effective viscosity, η_{eff}, is defined by a Newtonian and a plastic term as

$$\frac{1}{\eta_{\mathrm{eff}}} = \frac{1}{\eta_{\mathrm{N}}} + \frac{1}{\eta_{\mathrm{yield}}} \tag{4}$$

where

$$\eta_{\mathrm{yield}} = \frac{\tau_{\mathrm{yield}}}{2\dot{\epsilon_{\mathrm{II}}}} \tag{5}$$

with $\dot{\epsilon_{\mathrm{II}}}$ as second invariant of the shear strain rate (see also Schott & Schmeling 1998). Material yields plastically if the second (shear stress) invariant of τ, τ_{II}, reaches a critical τ_{yield}. This behaviour is approximated by determining η_{yield} such that $\tau_{\mathrm{II}} < \tau_{\mathrm{yield}}$ at all times. To mimic the brittle behaviour of a fault-filled crust τ_{yield} is calculated from a Coulomb friction law for optimally oriented faults

$$\tau_{\mathrm{yield}} = (a\sigma_{\mathrm{n}} + b)\lambda \tag{6}$$

with a and b denoting constants, σ_{n} for the normal stress, and the pore pressure factor

$$\lambda = 1 - \frac{p_{\mathrm{pore}}}{p_{\mathrm{lith}}}, \tag{7}$$

which describes the fluid pore pressure, p_{pore}, of the lithosphere relative to the lithostatic pressure

$$p_{\mathrm{lith}} = \rho g z. \tag{8}$$

Here, z denotes depth and g the magnitude of **g**. The λ factor is poorly constrained in nature and used as a constant, adjustable parameter for slab weakening in our models (3.1). For simplicity we assume $\sigma_{\mathrm{n}} = p_{\mathrm{lith}}$.

The viscosity of the slab, $\eta_{\mathrm{N}}^{\mathrm{slab}}$, is always set to a constant multiple of the upper mantle viscosity to approximate mechanical differences between the subducting plate and mantle which are of thermal and chemical origin in nature. The mantle viscosity jumps from its reference value in the upper mantle, $\eta_{\mathrm{N}}^{\mathrm{um}}$, to a higher value, $\eta_{\mathrm{N}}^{\mathrm{lm}}$, in the lower mantle. In this way, we capture the effect of an increase in viscosity in the lower mantle which is well documented and commonly associated with the 660 km phase transition (e.g. Hager 1984; Mitrovica & Forte 1997). However, we neglect other possible effects of phase transitions, for instance those related to a negative Clapeyron slope of the ringwoodite → perovskite + magnesiowüstite transition (e.g. Christensen 1996; Tetzlaff & Schmeling 2000). Table 1 lists all the parameters and the value (ranges) we have used in our models.

We solve eqs (1) and (2) in two dimensions using a stream function approach. The finite-difference (FD) code FDCON by Schmeling & Marquart (1991) is used with a resolution of 101 × 301 gridpoints for a model geometry (Fig. 1) with aspect ratio of 1 × 3 spanning a depth–width range of 1320 × 3960 km. Compositional differences between slab and mantle are treated by a tracer advection method; we use 800 × 2400 markers, which are initially roughly evenly distributed. Model results were found to be stable with respect to increasing resolution, both in terms of FD grid and marker number.

Mechanical conditions are free slip, impermeable on the top and bottom boundaries. Side boundaries are either treated as reflective (free slip) or periodic (e.g. Gottschaldt 1997) to explore the effect of constrained mantle flow (Section 3.2). In all models, the stream function was set to a constant, zero value at the top and bottom implying zero net horizontal flow. Thus, our box reference frame, which we used for calculations, corresponds to the centre of mass reference frame by Han & Gurnis (1999). To obtain a net horizontal flow in the box, one could add a constant horizontal velocity to the whole model. This would lead to an identical solution of the momentum equation.

The initial slab configuration was prescribed asymmetrically to facilitate the development of subduction on the one side of the plate as shown in Fig. 1. The oceanic plate away from the trench was detached from the side boundaries ('free slab') for all periodic boundary condition (BC) models. For reflective boundary conditions the oceanic plate away from the trench was either detached from the side boundaries or it was attached to the side wall ('fixed slab'). We note that periodic free slabs cannot be pinned in this fashion because this would imply overconstrained mechanical BCs, namely

Table 1. Model parameters.

Quantity	Symbol	Value (range)	Source
Cohesion	b	60 MPa	Byerlee (1978) for $z < 40$ km
Density contrast between slab and mantle	$\Delta\rho\|_{\mathrm{slab}}$	50 kg m^{-3}	
Domain height		1320 km	
Domain width		3960 km	
Friction coefficient	a	0.6	Byerlee (1978) for $z < 40$ km
Gravitational acceleration	g	10 m s^{-2}	
Pore pressure factor	λ	0.01–1	
Thickness of the slab	d	66–99 km	
Viscosity of the mantle	$\eta_{\mathrm{N}}^{\mathrm{m}}$	$\eta_{\mathrm{N}}^{\mathrm{um}}$ for $z < 660$ km	
		$\eta_{\mathrm{N}}^{\mathrm{lm}} = 50\eta_{\mathrm{N}}^{\mathrm{um}}$ for $z \geq 660$ km	
Viscosity of the slab	$\eta_{\mathrm{N}}^{\mathrm{slab}}$	100–500 $\eta_{\mathrm{N}}^{\mathrm{um}}$	
Viscosity reference (upper mantle)	$\eta_{\mathrm{N}}^{\mathrm{um}}$	10^{20} Pa s	

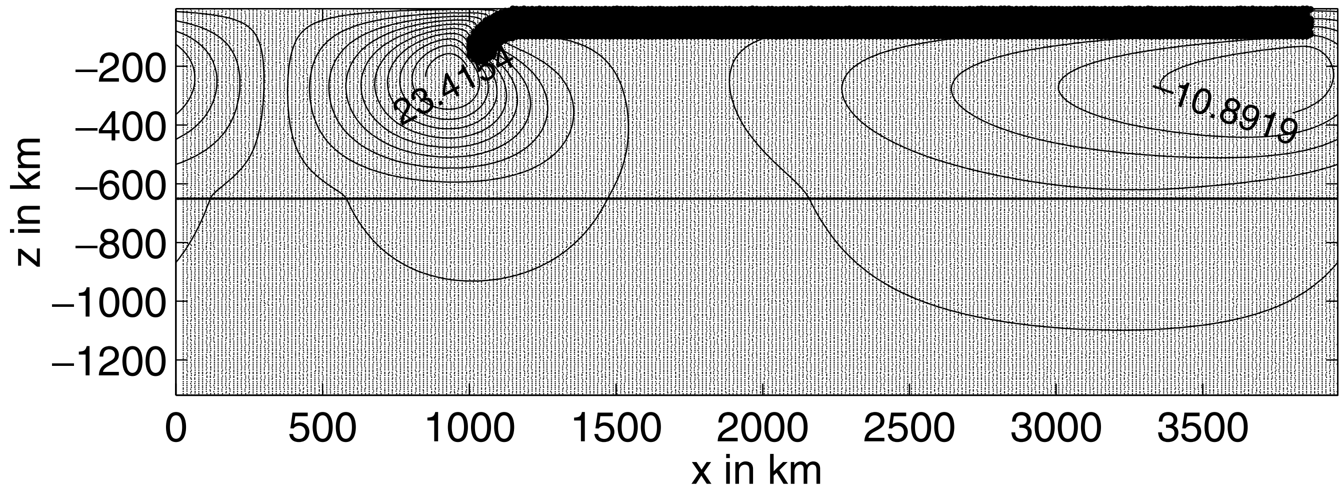

Figure 1. Initial distribution of tracers for a free slab model and periodic boundary conditions. We show every eighth and fourth tracer in horizontal and vertical direction, respectively. Contour lines denote stream-function isolines with selected annotated contours. Non-dimensional stream function values of 1 correspond to 10^{-5} m^2 s^{-1}.

fixing one particular point of the slab to the net horizontal velocity of the whole model. Thus, all models with periodic BCs have a free slab.

3 RESULTS

3.1 The trench decoupling mechanism

Before discussing the time dependence of subduction and trench motion for different boundary conditions we explore the role of plastic 'Byerlee' yielding. For viscous flow models it is difficult to initiate and obtain slab-shaped downwellings without describing a trench geometry (e.g. King & Hager 1990; Conrad & Hager 1999) or surface velocities (e.g. Christensen 1996). To avoid having blob-type slabs dominated by Rayleigh–Taylor instability, we choose to augment a purely viscous rheology with yielding in an attempt to mimic faulting in the brittle deformation regime of the uppermost lithosphere (eq. 4). Depending on the yielding parameters, there are large differences in the slab shapes and the time needed for the downwellings to reach mid-mantle depths. Fig. 2 shows models at roughly the same state of subduction for different choices of the pore pressure factor λ.

The maximum depth of the slab versus time is shown in Fig. 3 to illustrate the time dependence of the downwelling flow that is associated with the models shown in Fig. 2. For the dry, $\lambda = 1$, case a Rayleigh–Taylor instability forms and the dense material sinks slowly into the mantle while thinning at mid to upper mantle depths, indicating a resistance of the uppermost slab material to detach from the free-slip surface.

The sinking velocities as indicated by Fig. 3 are slower for $\lambda = 1$ than for the weak yielding case of $\lambda = 0.1$. These differences are caused by changes in the effective slab viscosity (eq. 4), which is unaltered in the bending region but slightly lower at the trench with $\sim 70\eta_N^{um}$ for $\lambda = 1$. The $\lambda = 0.1$ case is characterized by a well-defined slab and little intraslab deformation. The bending region of the slab attains an effective viscosity of $\sim 50\eta_N^{um}$, with a minimum of $\sim 10\eta_N^{um}$ at the decoupling zone. The viscosity of the plate part, which is not subducted, is reduced on the surface to $\sim 80\eta_N^{um}$ for depths of $z < \sim 20$ km. The subducted part of the slab is not weakened for $z > \sim 200$ km.

In contrast, $\lambda = 0.01$ leads to a strong weakening and slab thinning in the trench region with eventual slab tear-off at the surface. Viscosities at the trench are lower than those of the upper mantle ($\sim 0.05\eta_N^{um}$). The stiffness of the bending region is strongly reduced to $\sim 30\eta_N^{um}$ during the initial subduction stage before slab tearing. The subduction velocity is moderately faster than for larger λ values (Fig. 3), indicating a strong control of the weakening mechanism at the trench which would be enforced by power-law rheology.

From this comparison of different Byerlee strengths we choose $\lambda = 0.1$ for the models below, since the slab detaches freely from the surface and roughly retains its thickness without necking. The choice of $a\lambda$ is consistent with the range of values for the friction coefficient, which could be applicable to the subduction zones on Earth, given, for example, by Moresi & Solomatov (1998). Without a brittle lithosphere or with high values of $a\lambda$ Moresi & Solomatov (1998) did not observe mobile lid convection in their models. Furthermore, in the numerical experiments of Schott & Schmeling (1998) delamination and detachment of the mantle lithosphere occurred only if the lithosphere was weakened. Reasonable sinking velocities of the lithospheric root were obtained for λ values of ~ 0.07. In accordance with these models, the weakening of the lithosphere in our experiments is necessary to detach the slab from the surface and to allow the plate to move freely. Varying other parameters at fixed a, b and λ, we expect that the dynamics of subduction will be controlled by viscous slab bending and the interaction of the slab with mantle flow in a stratified viscosity setting, and not the upper boundary condition (*cf.* Funiciello *et al.* 2003a).

3.2 Stratified mantle subduction: influence of boundary conditions

Fig. 4 shows the development of subduction for our reference model with $\lambda = 0.1$, a slab thickness of $d = 99$ km and a stiffness of $\eta_N^{slab} = 100\ \eta_N^{m}$ for three different settings: free slab for periodic and reflective BCs, and fixed slab for reflective BCs. The natural analogue for these different end-member settings would be an oceanic plate which is relatively short and weakly coupled to a ridge, with flow determined by the plate alone (Fig. 4a) or with restricted flow, possibly due to neighbouring subduction zones or large-scale convective currents (Fig. 4b). Fig. 4(c) would correspond to subduction on the

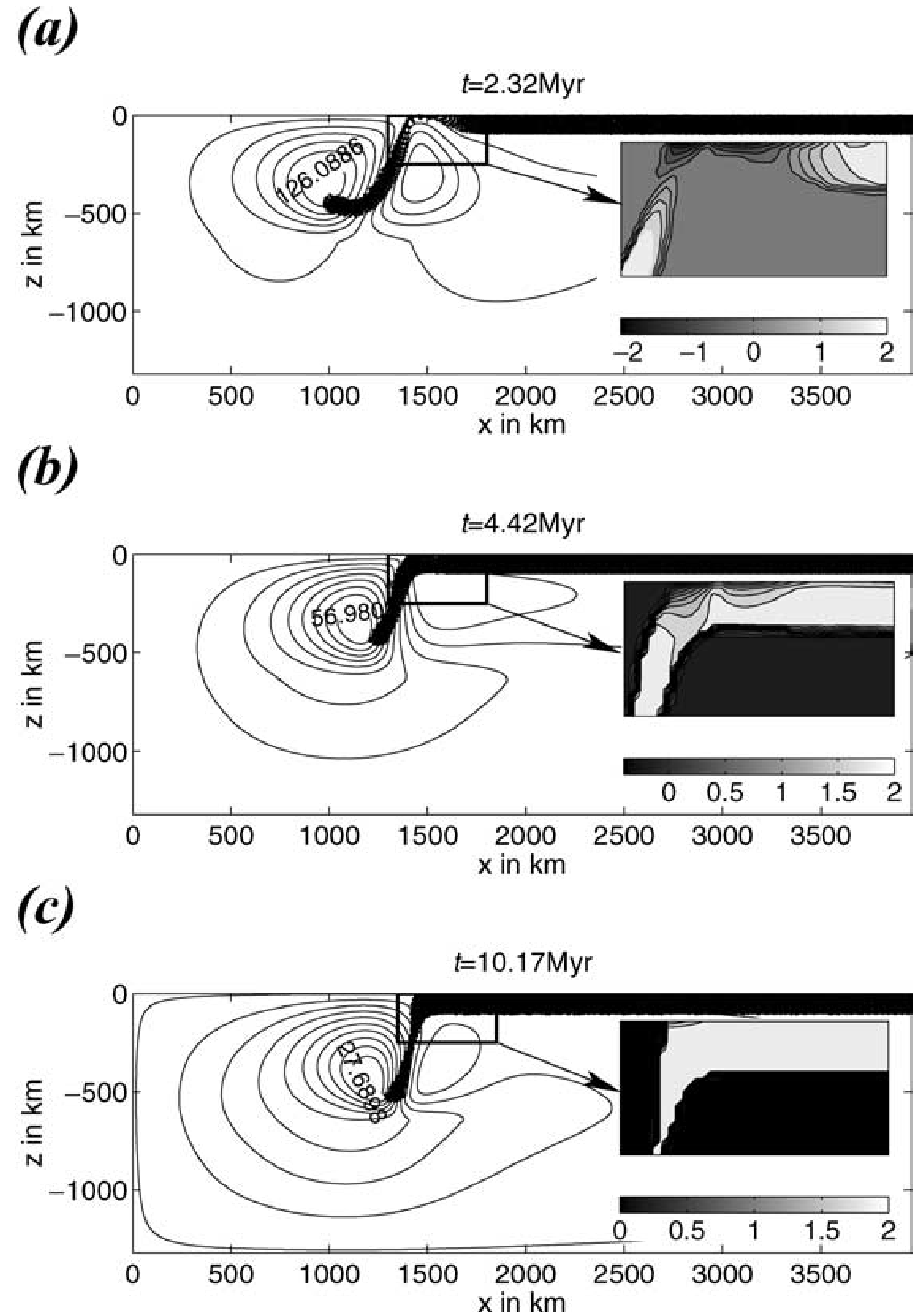

Figure 2. Snapshots of subduction for a fixed slab with reflective boundary conditions for pore pressure factors $\lambda = 0.01$ (a, at time $t = 2.32$ Myr), $\lambda = 0.1$ (b, $t = 4.42$ Myr) and $\lambda = 1$ (c, $t = 10.17$ Myr). The thickness of the slab is $d = 99$ km and $\eta_N^{\rm slab} = 100\ \eta_N^{\rm m}$. This plot is similar to Fig. 1 but only slab material tracers are shown. Inset figures in the upper right corners show $\lg(\eta/\eta_{\rm um})$ near the slab bending region. Dark shading indicates low viscosity and light shading high viscosity. (In the colour online version blue is low and red high viscosity.)

side of a plate which is relatively large and slowly moving, such as slabs in the central Mediterranean attached to the African Plate. For Fig. 4(c), all subduction has to be taken up by in-slab deformation and rollback.

The time dependence of several subduction features for the models shown in Fig. 4 are compared in Fig. 5.

3.2.1 Slab folding

We can distinguish different slab morphologies and flow patterns due to the interaction of the sinking slab with the 660 km viscosity contrast. All models show slab flattening and a reduction in the subduction velocity once the slab notices the viscous drag effect of the lower mantle during its descent (at $t \sim 5.5$ Myr). Part of the subduction motion is always taken up by oceanward trench rollback; in the case of the fixed slab (Fig. 4c), this is simply a consequence of conservation of mass. Note also that the free slab model shows the development of a second downwelling to the right of the subducting plate as a viscous instability for times larger than $t \sim 12$ Myr (Figs 4a and b).

We observe folding of the slab at depth, an effect that is most pronounced for the reflective free slab (Fig. 4b) but is also a

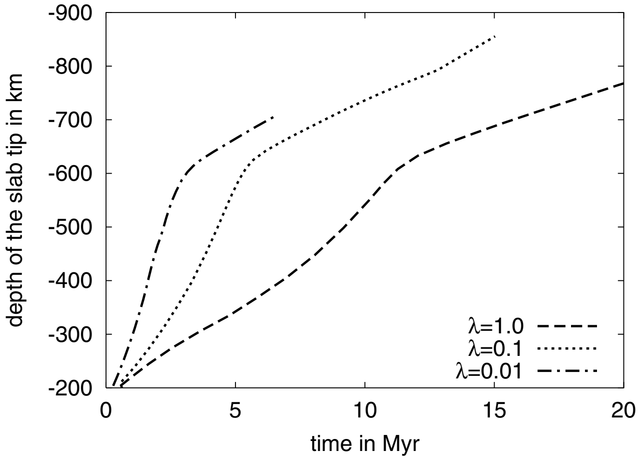

Figure 3. Maximum depth of slab, $z_{\rm slab}$, for the fixed slab models of Fig. 2 versus time, t, for pore pressure factors of $\lambda = 0.01$, 0.1 and 1.

prominent feature of the fixed slab (Fig. 4c). No folding is observed for periodic BCs (Fig. 4a). The basic difference between periodic and reflective side boundaries is that the descending slab can introduce a relative current in the lower mantle and 'push' material to the side for periodic BCs. Thus periodic BCs increase the horizontal mobility of the lower mantle and allow lateral movement of the trench relative to the position of the slab material, which slowly penetrates into the lower mantle with the result that there is no folding (Fig. 4a). If, due to lateral confinement of mantle material at the box sides, the trench position overlies the point of lower mantle penetration for some time as in Fig. 4(b), the difference between upper and lower mantle subduction velocities results in folding. This condition is still met in the fixed slab case, as can be verified by inspecting Fig. 4(c). Indeed, combining Figs 5(b) and (c) reveals that the folding cases are characterized by slow trench retreat velocities relative to the lower mantle, while the non-folding case has a higher (3–4 cm yr^{-1}) retreat velocity at the late stages. This finding is corroborated by additional experiments we performed for a fixed slab with reflective BCs and larger aspect ratios (not shown). There, folding is also reduced compared with the models with a smaller aspect ratio since a slab with a larger aspect ratio allows a larger differential velocity between the trench and lower mantle.

Slab folding can be understood as a viscous instability, the growth rate of which depends on the viscosities of the mantle and plate, the plate thickness and the layer (or slab) parallel compressive force (e.g. Turcotte & Schubert 1982, p. 262). For a sinking slab that encounters a viscosity contrast, the compression parallel to the slab is higher for a vertical than for an inclined slab, because the latter can 'push' the lower mantle material to the side. Therefore, there is no folding if the subduction velocity contains a significant component parallel to the mobility of the lower mantle and/or if the viscosity and thickness of the slab are large. An increased lower mantle viscosity decreases its mobility, raises the compressive force parallel to the slab, and hence leads to larger folding tendency.

3.2.2 *Interaction with the 660 km boundary and rollback*

From the maximum depth of the slab, $z_{\rm slab}(t)$, in Fig. 5(a), we can observe two stages of subduction, before and after the effect of the 660 km boundary and sluggish lower mantle flow is felt by the downwelling (*cf.* Funiciello *et al.* 2003a, and compare our Fig. 3). Differences in $z_{\rm slab}(t)$ between BCs for the free slab setting are small, while the fixed slab descends at slightly lower speeds. Absolute

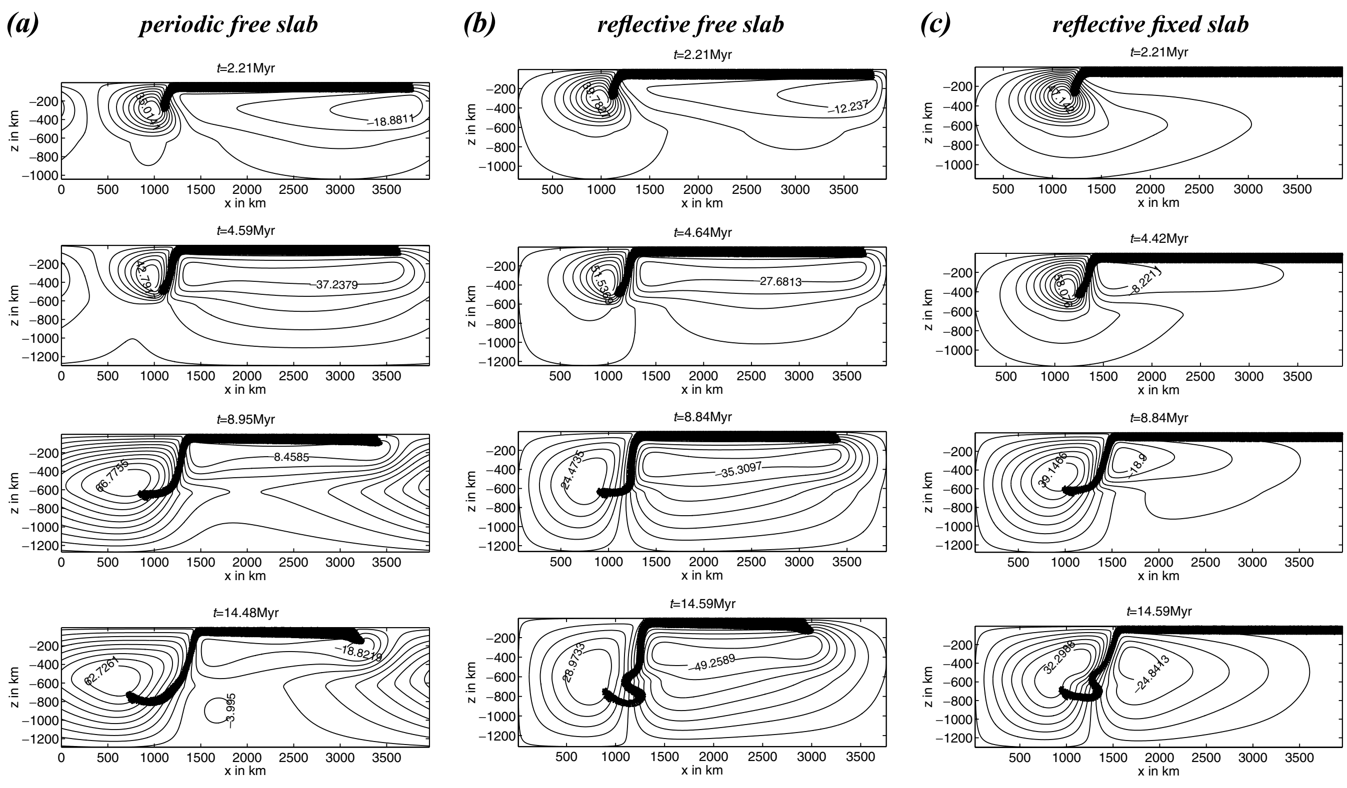

Figure 4. Reference subduction models ($d = 99$ km, $\eta_{\rm N}^{\rm slab} = 100\ \eta_{\rm N}^{\rm um}$) for a free slab with periodic boundary conditions (BCs) (a), a free slab with reflective BCs (b), and a fixed slab with reflective BCs (c). For the time dependence of several variables see Fig. 5. Models shown here and in Figs 6 and 8 have $\lambda = 0.1$.

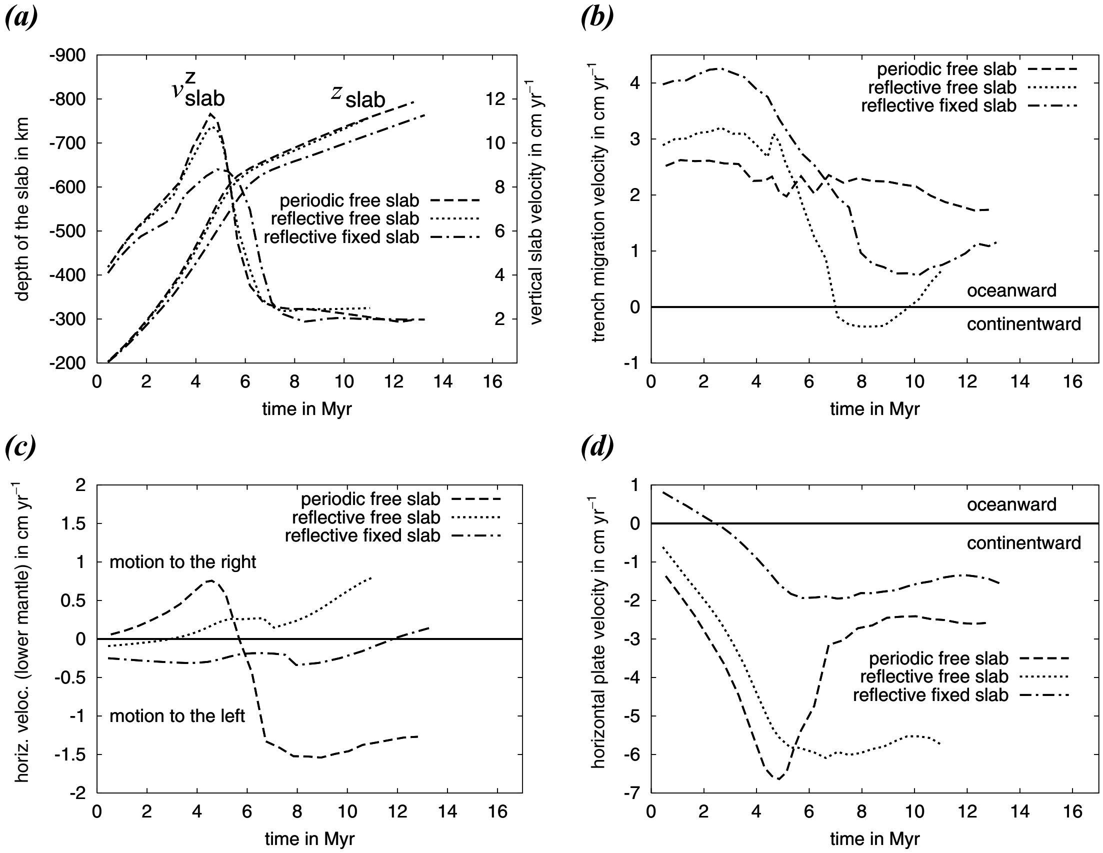

Figure 5. (a) Maximum depth of slab, $z_{\rm slab}$, and vertical velocity of the lowermost part of the slab, $v^z_{\rm slab}$ (defined as the maximum z coordinate of the deepest tracer in the lowermost part of the slab, velocity derived from the z curve); (b) trench velocity, $v_{\rm t}$ (defined by 11 tracers at the trench on the top of the model box); (c) mean horizontal motion of the lower mantle, $\langle v^h_{\rm lm}\rangle$ (defined as average horizontal velocity at the gridpoints in the lower mantle); (d) horizontal velocity of the oceanic plate at the surface, $v_{\rm p}$ (defined as average velocity at the gridpoints in the oceanic plate at the surface), all against time. Lines indicate a free slab with periodic BCs (dashed in the print version; red in the online version), a free slab with reflective BCs (dotted; green) and a fixed slab with reflective BCs (dot-dashed; blue); compare with Figs 4(a), (b) and (c), respectively.

values of subduction velocities are of the order of $\sim$10 cm yr^{-1}. We discuss how the time dependence of subduction might be influenced by neglected mechanisms which were not included in our models in Section 4.1.

The second stage of subduction is near to steady state and characterized by roughly constant subduction and plate velocities (Figs 5a and d), in contrast to acceleration of the slabs in the upper mantle.

A greater difference for the three initial and boundary condition settings is displayed by the trench velocities, shown in the box reference frame in Fig. 5(b). For reflective boundary conditions, oceanward rollback is steady initially and then reduced substantially once the slab comes close to 660 km, where escape flow has to be increasingly channelled through the stiffer lower mantle.

As expected, at least for the initial stage, the fixed slab model has larger rollback velocities than the free models. However, the ponding of the fixed slab on the 660 km boundary leads to flow confinement and folding of the slab, which strongly slows down retreat of the trench. The initially faster rollback rates of the fixed slab become slower than the rollback speeds of the periodic free slab at $\sim$6 Myr. The flow confinement imposes a rather strong constraint so that the rollback velocity of the fixed slab becomes significantly less than the subduction velocity (compare Figs 5a and b). This can only be accomplished by significant stretching of the lithosphere and slab (*cf.* Fig. 4c versus Figs 4a and b).

The model with periodic BCs displays a slow retreat throughout the model run (Fig. 5b), without much rate variation and no clear effect of the 660 km viscosity jump. This can be attributed to the ability of the slab to induce a net flow in the lower mantle (Fig. 4).

3.3 Influence of slab properties

3.3.1 Stiff slab

To illustrate the effect of a stiffer slab with $\eta^{\rm slab}_{\rm N} = 500\ \eta^{\rm m}_{\rm N}$, we show additional model snapshots in Fig. 6 and the corresponding time dependence of the model parameters in Fig. 7. Subduction is slower than for the reference model of Fig. 4, and the slab reaches 660 km at $\sim$8 Myr, roughly 2 Myr later than for $\eta^{\rm slab}_{\rm N} = 100\ \eta^{\rm m}_{\rm N}$ (Fig. 7a). The viscous bending of the slab at the trench dominates the models initially and causes a lower speed of subduction (*cf.* early stages of Figs 5a and 7a). In addition to the slab morphologies, which are different for the ponding stage, we therefore also find a dependence of subduction velocities on slab viscosity during the first stage of slab descent. This difference is, however, not as large as in the case of slab viscosity being the only property controlling subduction (Becker *et al.* 1999a; Funiciello *et al.* 2003a,b), indicating an important effect of mantle currents even at the early stages of subduction. Once the bending is overcome and subduction fully developed, the mantle

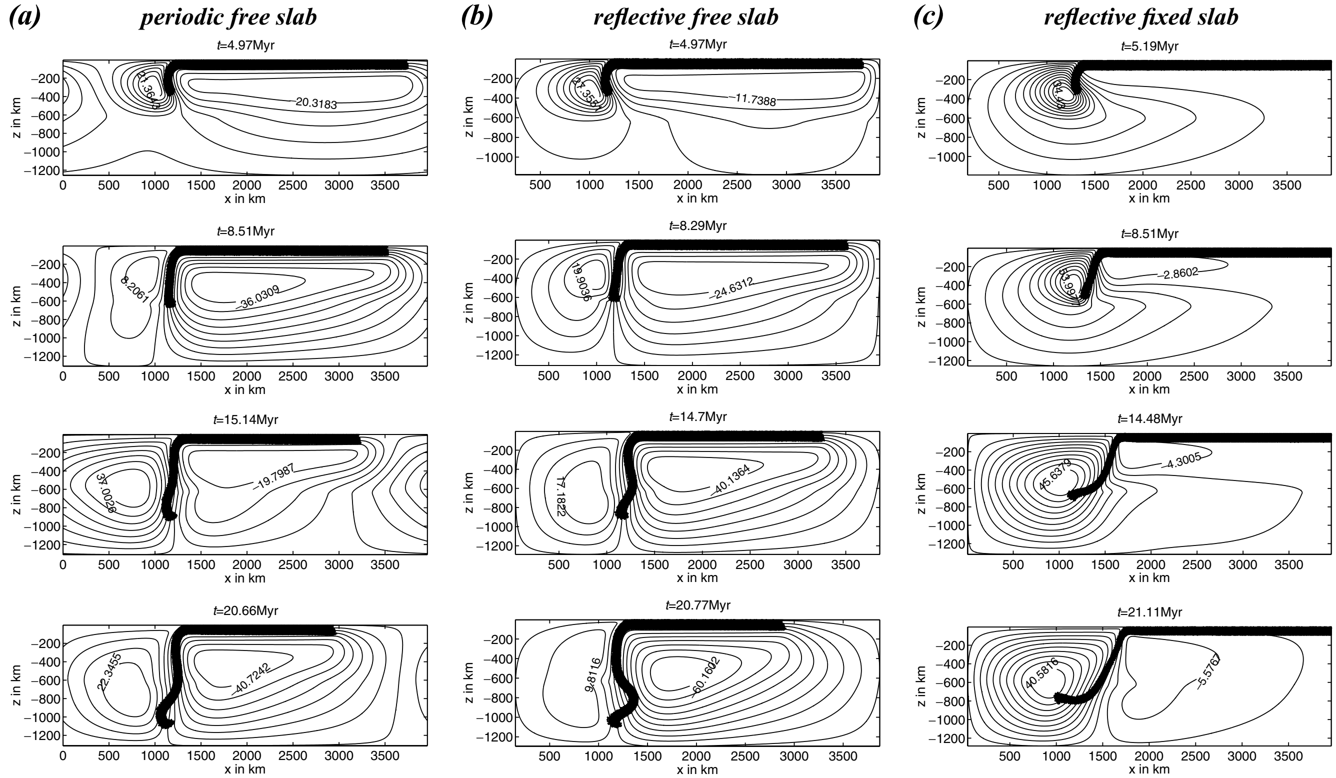

Figure 6. Stiff slab model ($d = 99$ km, $\eta_N^{slab} = 500\,\eta_N^{um}$) for a free slab with periodic BCs (a), a free slab with reflective BCs (b), and a fixed slab with reflective BCs (c) as in Fig. 4. For the time dependence of several variables see Fig. 7.

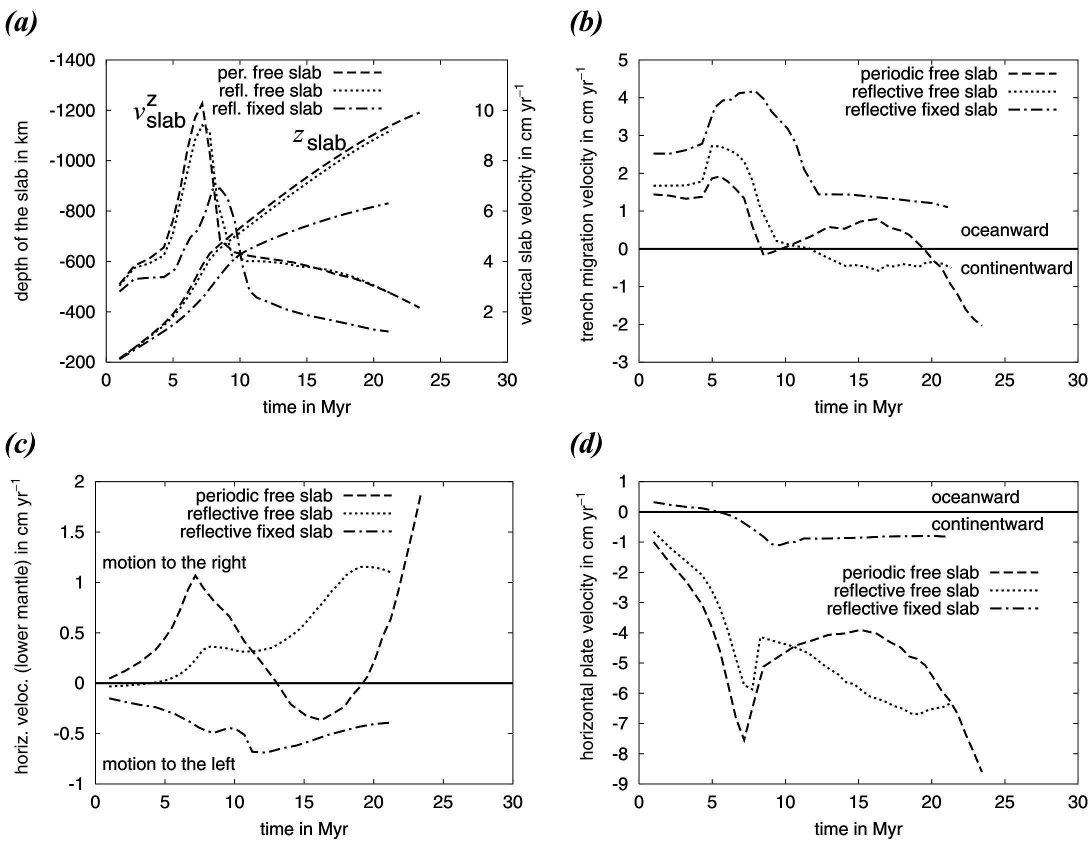

Figure 7. For a stiff slab: (a) maximum depth of slab, z_{slab}, and vertical velocity of the lowermost part of the slab, v^z_{slab}; (b) trench velocity, v_t; (c) mean horizontal motion of the lower mantle, $\langle v^h_{lm}\rangle$; and (d) horizontal velocity of the oceanic plate at the surface, v_p (as in Fig. 5) for the stiff slab model of Fig. 6.

drag appears to dominate, and the peak of the subduction velocity is only slightly lower than for smaller slab viscosity. (Figs 5a and 7a, 5–10 Myr).

On the one hand, the folding tendency for all BCs is reduced in the sense that undulations in Fig. 6 are of longer wavelength and slower folding growth rates than in the reference slab in Fig. 4, consistent with a viscous instability. Accordingly, we also do not see the development of Rayleigh–Taylor-type de-blobbing on the left plate edge as was found in Fig. 4(a), (b) for the stiff slab during the model run. On the other hand, stiff slabs for Fig. 6(a) penetrate more steeply into the mantle (*cf.* Davies 1995) and are not slowed down by the lower mantle as much. The subduction velocity of the deepest part of the slab after slab penetration into the lower mantle reduces to about a half of its maximum value compared with about a quarter of the maximum velocity value for the reference slab (Figs 5a and 7a). The steep subduction leads to two well-defined convection cells around the slab, comparable to the reflective boundary condition case of Fig. 4(b). Accordingly, the folding tendency increases in the periodic free slab in Fig. 6(a), and some undulations in the retreat, lower mantle and plate velocities are visible in Figs 7(b), (c) and (d), respectively. The fixed slab no longer show any folding instability (Fig. 6c). This is due to the reduced lithosphere stretching compared with the reference model (Fig. 5d), displacing the trench from the position of lower mantle penetration.

The different trench motion behaviour depends on how the slab transmits forces and momentum to the lower mantle. Stages of pushing the lower mantle relatively forward and backward alternate (Fig. 7c), and the backward bending, more common for stiff slabs, is related to continentward trench motion. Compared with the reference slab, the free stiff slabs always have slower oceanward trench retreat velocities than the fixed stiff slab. As Fig. 7(c) shows, the initially steeper descent for the stiff slab (compare Figs 6a and b) leads to more similar lower mantle currents for periodic and reflective BCs, implying that the slab is not able to exert a significant net push on the lower mantle within the first 20 Myr. Only at a late stage (25 Myr) does the backward-bent subducting slab within the upper mantle, in combination with periodic BCs (not shown), accelerate the trench to continentward velocities of over 2 cm yr^{-1}. The mechanism for the excitation of lower mantle flow is therefore dependent on slab rheology, the steepness of subduction through the upper mantle and the details of interaction with the 660 km boundary.

3.3.2 *Thin slab*

A thin subducting slab is shown in Figs 8 and 9, corresponding to a younger slab where the hypothetical isotherm defining the cold, oceanic lithosphere would have had less time to diffuse into the mantle. For the thin slab, the contrast in rheology between slab and mantle is less important for the overall flow characteristics. Rather, the mantle flow strongly shapes the slab. This is shown, for instance, in the pronounced formation of a 'mushroom' shape at the slab tip after interaction with the higher-viscosity lower mantle; a feature commonly seen in models of sinking density anomalies in only radially stratified media (e.g. Kárason 2002, for a slab application). The thin slab is also more easily bent, leading to strong folding for all boundary conditions displayed in Fig. 8.

Compared with the reflective free and fixed slabs the trench retreat for the thin periodic free slab is the slowest initially and the fastest finally, as was observed for the reference models. But in contrast to the reference models the trench retreat of all thin slabs is not constant during the first 4 Myr but increases steadily before interaction of the slab with the lower mantle (Figs 5b and 9b). There

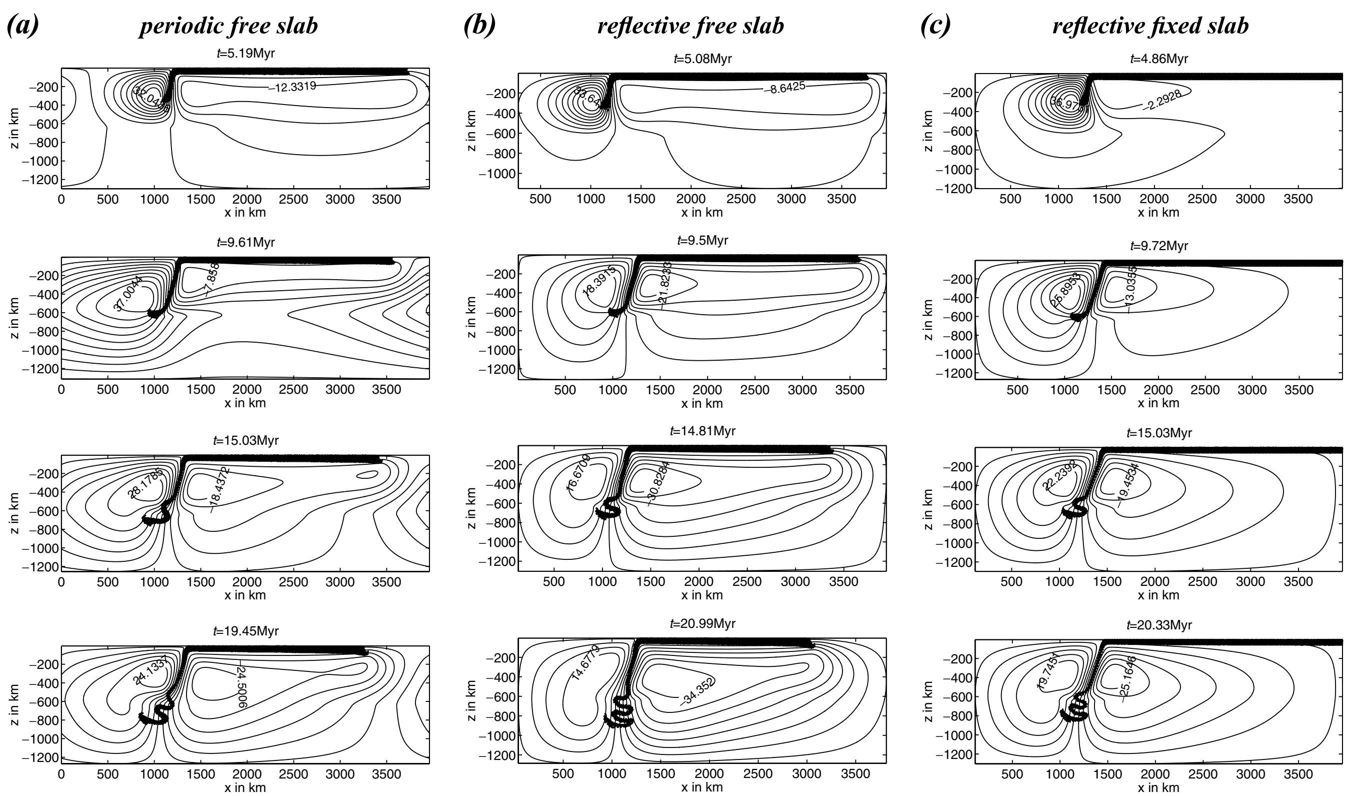

Figure 8. Thin slab model ($d = 66$ km, $\eta_N^{\mathrm{slab}} = 100\ \eta_N^{\mathrm{um}}$) for a free slab with periodic BCs (a), a free slab with reflective BCs (b) and a fixed slab with reflective BCs (c) as in Fig. 4. For the time dependence of several variables see Fig. 9.

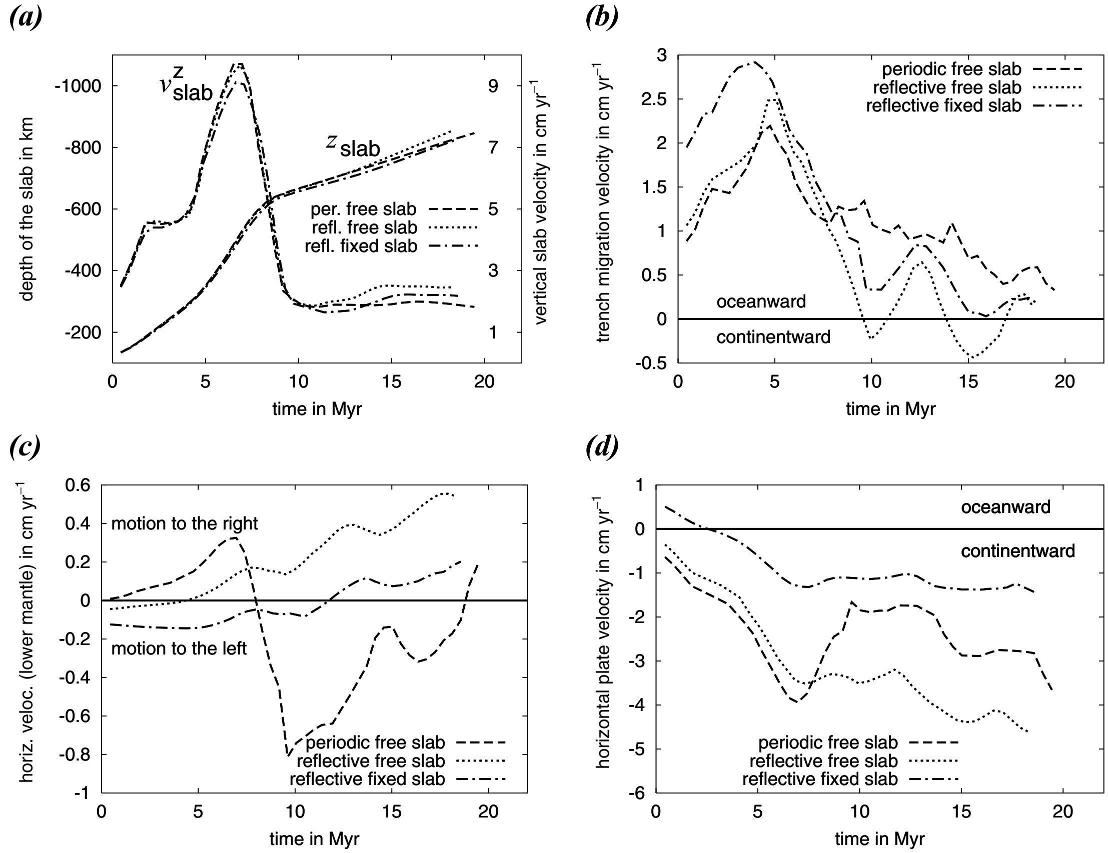

Figure 9. For a thin slab: (a) maximum depth of slab, z_{slab}, and vertical velocity of the lowermost part of the slab, v^z_{slab}; (b) trench velocity, v_t; (c) mean horizontal motion of the lower mantle, $\langle v^h_{\mathrm{lm}} \rangle$; and (d) horizontal velocity of the oceanic plate at the surface, v_p (as in Fig. 5) for the thin slab model of Fig. 8.

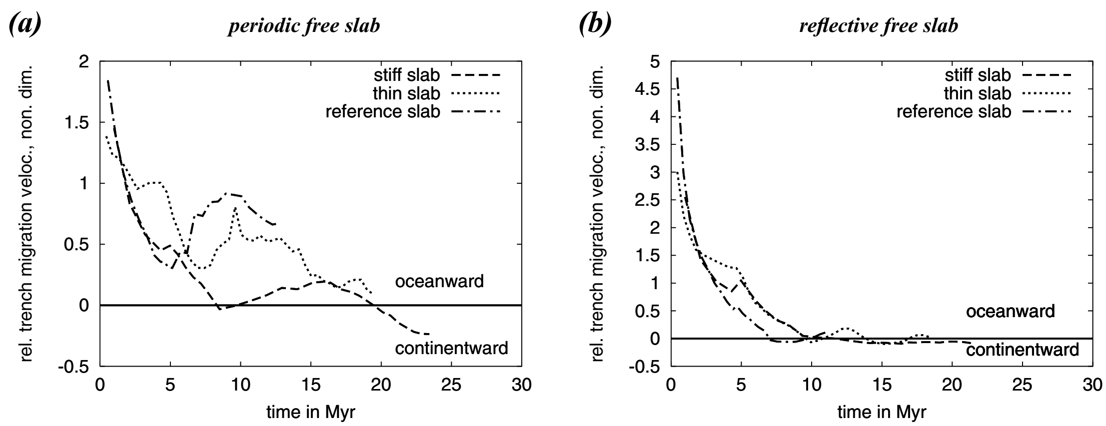

Figure 10. Relative trench migration velocities for free periodic and reflective slabs.

is also some increase of the trench retreat seen for the stiff slab (Fig. 7b). The early stage of subduction in the models is influenced by the prescribed dipping edge of the plate at the beginning of the model run. The slab shows increasing and then constant subduction velocity until ~4 Myr (Fig. 9a), which is caused by the decreasing bending radius and weakening of the bending region. If a certain geometry and rheology of the slab is reached the slab descent is no longer influenced by the initial slab shape.

The behaviour of the periodic and reflective free slabs is similar initially, and after the interaction with the 660 km boundary the trench retreat velocity shows stronger undulations for the reflective slabs than for periodic ones.

3.4 Relative trench migration velocity

Some systematics of the trench migration velocity can be inferred from the models when distinguishing between different subduction stages. Figs 10(a) and (b) show the trench migration velocities, v_t, normalized by the plate velocity, v_p, for the models with free slabs discussed above. We call this quantity the relative trench migration velocity (RTMV). For the fixed plate we cannot define the RTMV in this manner because of the very low plate velocities.

3.4.1 Periodic free slabs

The early stage of subduction is characterized by an initially high RTMV (retreat velocity up to twice the plate velocity), which rapidly decreases until the slab starts to interact with the 660 km boundary. As the slabs begin to penetrate into the lower mantle, increasing resistance slows down subduction velocities. As a result the relative retreat velocities increase again, reaching values as high as 0.8. At late stages, however, RTMV decreases again, probably because the surface part of the plates becomes small. Altogether, at intermediate or late stages of subduction, our periodic free slab models predict trench retreat velocities having a substantial fraction (0.4 ± 0.3) of the plate velocities.

3.4.2 Reflective free slabs

During the early stages of subduction, the RTMV curves are roughly similar to the periodic free slabs and the trench migration velocity exceeds the plate velocity by several times. However, at later stages the reflective free slabs experience stronger lateral constraints than the periodic slabs, which results in significantly smaller, almost negligible, RTMVs after interaction with the 660 km boundary.

4 DISCUSSION

4.1 Model limitations

Amongst the effects we have neglected in our model are, in perceived order of increasing importance, sphericity, elasticity, temperature diffusion, phase boundary effects other than increase in viscosity, lateral viscosity contrasts in the mantle (possibly due to an asthenospheric channel below the oceanic plate), power-law rheology and 3-D, time-dependent flow effects.

The average viscosity of a subducting plate is subject to debate. Rheological laws determined in the laboratory (e.g. Ranalli 1995) would predict very stiff slabs. However, many features of subduction zones can be explained with fluid models (e.g. Vassiliou & Hager 1988; Tao & O'Connell 1993; Zhong & Gurnis 1994), and seismically determined strain rates within slabs are comparable to the ambient mantle (Bevis 1988). This implies an effective weakening of the slab relative to a simple temperature-dependent rheology (*cf.* Čížková *et al.* 2002). Furthermore, the viscosity of the subducting slab at the trench may be important in controlling slab dynamics. Models find the upper limit of effective trench viscosities of the subducting plate to be $\sim 10^{23}$ Pa s (Conrad & Hager 1999; Becker *et al.* 1999a).

The effectiveness of diffusion to weaken the temperature-dependent slab viscosity will depend on the local Peclet number and, while probably small, can be expected to reduce slab viscosity somewhat before slabs reach 660 km. Large bending strain rates can lead to slab weakening in the trench region if a power-law rheology is active at shallower depths in the lower-temperature mantle. Both strength-reduction effects can be expected to accelerate subduction, as is also shown by the varying yield stress models of Figs 2 and 3.

An asthenospheric lower-viscosity region, which might exist under oceanic lithosphere, would furthermore speed up our subduction velocities, as the amount of drag underneath the horizontal part of the plate would be reduced. Since driving forces and stresses scale only with the slab-pull density contrast $\Delta\rho|_{\mathrm{slab}}$, model velocities are inversely proportional to $\eta_{\mathrm{N}}^{\mathrm{um}}$ and increase linearly with $\Delta\rho|_{\mathrm{slab}}$. As our simplified model does not include these accelerating ingredients, we have chosen to scale it with 10^{20} Pa s as an effective mantle viscosity (Table 1). If we use the canonical viscosity value of 10^{21} Pa s from post-glacial rebound for the upper mantle instead, the subduction velocities shown in Figs 5, 7 and 9 would be lower by a factor of ten.

The effect of the 410 km and 660 km phase transitions, which have both been neglected in terms of the associated density changes, has been discussed extensively (e.g. Christensen 2001, for a review). While it is well established that the 410 km transition will have an accelerating effect on subduction, the effective Clapeyron slope of the 660 km transition might be almost zero (e.g. Weidner & Wang 1998), implying a small density effect. However, models that include phase change dynamics can be expected to show more episodicity in terms of rollback dynamics (e.g. Zhong & Gurnis 1995a).

4.2 Reference frames and net motions

While the net horizontal flow of the whole mantle has to be zero (Section 2), there may exist a mean horizontal velocity of the lower mantle for both periodic and reflective BC models. Only for the former case, however, does this motion correspond to a net motion of the lower mantle with respect to the lithosphere. For the latter, i.e. reflective boundary conditions, one has to take into account the mirror image with velocities opposite to the box which is actually modelled. Were we to average over this pair of cells, the net horizontal motion of the lower mantle would cancel out to zero. The excitation of net relative rotation motion between the upper and lower mantle for periodic boundary conditions is only possible for a laterally varying viscosity (Ricard *et al.* 1991; O'Connell *et al.* 1991) such as subduction of high-viscosity slabs.

Comparison of the induced lower mantle currents for different slab properties (e.g. Figs 5 and 7) demonstrates that the slab mechanism for excitation of net relative lower mantle motion which we described above will depend on the interactions of the slab with the 660 km rheological contrast. Net rotation induced by slab/660 km interaction could be invoked as an explanation for the observed net rotation in the hotspot reference frame. This hypothesis should be tested with global 3-D models. The relative net rotation of the lower mantle could also be caused by the continental roots, as was observed in the numerical experiments of Zhong (2001).

Since we are dealing with mean horizontal motions relative to the oceanic plate, we could define alternative reference frames for slab motion, specifically trench motion. Previously, we viewed velocities in a box-relative framework (e.g. Figs 5b and d) which in nature would have to be defined based on neighbouring convection cells. An alternative reference frame is with respect to a stable lower mantle, where we could subtract any total mean horizontal motion of the lower layer (Fig. 5c) from trench (Fig. 5b) and horizontal plate velocities (Fig. 5d) (*cf.* Garfunkel *et al.* 1986).

If we display trench migration velocities in the lower mantle and box reference frames for periodic and reflective free slabs (reference models, Fig. 11a and b), the difference between velocities in both reference frames is of the order of 10 per cent for reflective BCs. For periodic BCs the velocity in the lower mantle reference frame is about twice as high as in the box reference frame after interaction of the slab with the lower mantle.

Since we cannot incorporate the effect of other large-scale currents and subduction that will affect flow in nature (e.g. Steinberger & O'Connell 1998), our lower mantle reference frame would only

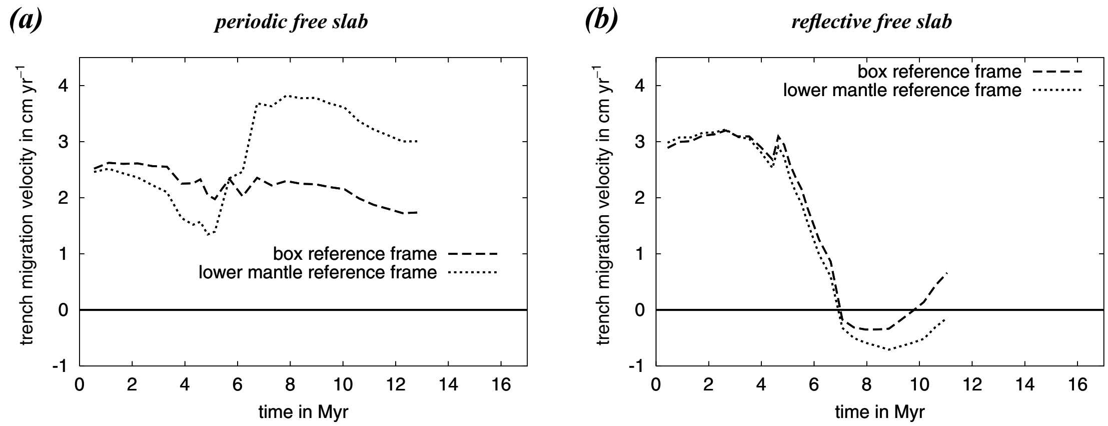

Figure 11. Trench migration velocities with respect to the lower mantle (v_t^{lm}) and to the model box (v_t^{b}) for reference model free slab, periodic BCs (a), and reference model free slab, reflective BCs (b). Compare with box reference-frame rates shown in Fig. 5b.

be a regional realization of a hypothetical lower mantle, hotspot reference frame on Earth. Therefore we used the box reference frame for all models (*cf.* Han & Gurnis 1999) while taking into account that the relative trench migration velocities for periodic BCs and the late subduction stage could be higher in the lower mantle reference frame.

4.3 Comparison with previous work

All of our models with stratified viscosity are characterized by a slowdown of subduction and ponding (*cf.* Gurnis & Hager 1988). If we increase the contrast between upper and lower mantle viscosity to larger values of ∼150, the vertical motion of the slab is strongly reduced and a long ponding stage results. Our findings on the deformed slab shapes at depth are consistent with earlier work that showed that phase transition dynamics (Zhong & Gurnis 1995a; Christensen 1996) and density or viscosity layering (Kincaid & Olson 1987; Gurnis & Hager 1988; Gouillou-Frottier *et al.* 1995; Griffiths *et al.* 1995; Christensen 1996) can produce a variety of ponded slab shapes at 660 km as a function of rollback. Furthermore, Gaherty & Hager (1994) showed that compositional contrasts in the slab can also lead to strong folding. However, we find that the various degrees of flow confinement to which 2-D models are limited (explored by periodic and reflective BC models) are important for determining the shape of a slab at depth (*cf.* Faccenna *et al.* 2001a,b). The choice of periodic BCs also leads to a shallower dip angle of the slab after its interaction with the viscosity contrast, as was observed by Gurnis & Hager (1988) and Han & Gurnis (1999). In our model framework, the various slab morphologies and the ponding of subducted material at or above the 660 km transition which are seen in seismic tomography (e.g. Fukao *et al.* 2001; Becker & Boschi 2002; Kárason 2002) would be explained as a function of the descent of dense material that interacts with a viscosity contrast, with the surface observable of various rates of trench rollback.

Amongst the effects that may determine the long-term fate of deep slab subduction, slab rollback and the effect of the phase transition are well studied (e.g. Christensen 2001). However, many of these models treat rollback as an input parameter (Gouillou-Frottier *et al.* 1995; Griffiths *et al.* 1995; Christensen 1996) and there are few studies which have focused specifically on the question of how trench motion is dynamically consistent with the slab dynamics (Kincaid & Olson 1987; Zhong & Gurnis 1995a), as we have striven to do here. The work of Zhong & Gurnis (1995a) is probably closest to our approach: for a cylindrical domain and a negative Clapeyron slope, those authors observed that slab rollback was strongest during the slab descent and the ponding phase on the 660 km boundary. Once material breaks through the phase boundary, trench motion was strongly reduced. We find a similar decrease in rollback velocities for our reflective boundary condition models where the sluggishness of flow in the lower mantle controls trench migration. However, for a certain range of slab parameters, our periodic BC models are either not affected by the 660 km boundary (box reference frame) or show re-acceleration after transient slowdown (lower mantle reference frame). It is difficult to compare our models with that of Zhong & Gurnis (1995a) because we have no negative Clapeyron slope. However, the convective currents in the cylindrical model of Zhong & Gurnis (1995a) may be more similar to our reflective case, consistent with the interpretation that rollback will be slowed down by confined flow.

The division of subduction into two phases (initial acceleration and slowdown after the lower mantle is felt) was also discussed extensively for laboratory analogue models by Faccenna *et al.* (2001b) and Funiciello *et al.* (2003a). Our numerical models for free oceanic plate subduction show behaviour similar to that in Funiciello *et al.* (2003a) for reflective boundary conditions. Again, boundary conditions are not exactly the same since the approach of Funiciello *et al.* (2003a) has a natural no-slip condition at the side walls. The source of episodicity for rollback in the analogue models was attributed to lateral, toroidal flow around the slab, which we cannot incorporate into our 2-D models.

4.4 What is the cause of rollback?

A consistent interpretation emerges from our models. If flow is confined by lateral material contrasts due to neighbouring slabs, convective cells or restricted flow through the lower mantle in 2-D numerical experiments with reflective boundary conditions, rollback is slowed down and the trench stagnates after interaction with the 660 km boundary. If there is the possibility of escape flow, laterally or by means of periodic boundary conditions in 2-D, rollback velocities are always a substantial fraction of the plate velocity. We conjecture that the physical reason for rollback lies in the minimization of the total dissipation rate of the flow driven by the subducting slab. This dissipation is partitioned into (1) a shear flow contribution that is induced by horizontal motion of the oceanic plate at the surface and

(2) a contribution due to the sideways-moving slab that is sticking into the mantle (i.e. the rollback contribution). For a given rate of change of potential energy due to subduction it appears that the rollback mode is often energetically favourable because it reduces dissipation due to shear flow (1) more than it increases dissipation due to roll back (2). Quantitative tests of this suggestion will be the subject of a future study.

4.5 Application to natural subduction zones

In terms of the general behaviour of subduction, our fixed slab, reflective boundary condition model (Fig. 4c) is most applicable to the central Mediterranean, where the small Calabrian slab is attached to the slowly moving, large African Plate. This setting has been discussed by Faccenna *et al.* (2001a), and our models are consistent with predicting rollback for this situation at a rate of about half the subduction rate. In addition to the apparent stagnation of the Calabrian slab above 660 km (e.g. Spakman *et al.* 1993; Piromallo & Morelli 2003), the presence of the Hellenic slab and remnant subduction also makes the Mediterranean a likely candidate for lateral flow confinement.

In the Marianas and the Tonga subduction zones, backarc spreading is observed, and the Tonga Trench in particular shows rapid rollback (Bevis *et al.* 1995). This setting where the Pacific Plate is moving rapidly towards the trench is more similar to our free slab cases (Figs 4a and b). There is also evidence for substantial deformation of the slab at depth (Giardini & Woodhouse 1986; van der Hilst 1995). These findings single out Tonga as a natural example for fast rollback with slab complexity at depth, possibly related to flattening and folding as observed for the periodic or reflective BCs case of our reference model (Fig. 4a or b, respectively). From these two models, only the periodic BC case has a relatively high normalized trench migration velocity of about 0.8 (Fig. 10).

In the Sunda arc, deep seismicity within the Wadati–Benioff zone appears to denote a tendency of the subducting slab to bend over backwards towards the oceanic plate at depth (e.g. Isacks & Barazangi 1977; Schöffel & Das 1999; Becker *et al.* 1999b). This slab behaviour might indicate that the compressional deformation state of the overriding plate at the surface (e.g. Jarrard 1986; Letouzey *et al.* 1990; Bock *et al.* 2003) is related to slab interaction with the 660 km boundary. Slabs with advancing trenches could potentially cause compression in an overriding plate. In our experiments, continentward trench motion is mostly seen for stiff slabs and reflective BC models and only after the slab reaches 660 km. A similar behaviour with advancing slabs after forward rolling on the 660 km boundary is also seen in laboratory experiments for certain parameter ranges (Faccenna *et al.* 2003a).

Seismic tomography has been used to argue for whole mantle style convection, accompanied by ponding and a range of slab morphologies at depth. This spurred the early geodynamic models which evaluated the effect of rollback on slab penetration. However, it is not clear if there is already (or if there will be in the near future) enough resolution to delineate folding of slabs, which previous geodynamic models and this study have documented as plausible behaviour in certain parameter ranges. Periodic boundary condition models, which allow for a greater amount of flow around the slab as would be expected in the 3-D Earth in general, are less likely to show folding. We should therefore consider simple, flat ponding as the more robust behaviour of slabs which interact with a viscosity jump. Indeed, quite complex slab images such as under the Sunda arc can plausibly be explained by the simple impingement of a weak (mantle viscosity) slab on a strong viscosity change with time-dependent trench motion (Kárason 2002).

Models such as ours that treat rollback consistently show that the shape of the slab depends quite critically on the large-scale mantle flow. Besides that, slab anomalies at depth will also be affected by the change in plate boundary configurations and plate velocities with time (Lithgow-Bertelloni & Richards 1998). If slab anomalies are furthermore advected laterally by mantle flow in such reconstructions of subduction history (Steinberger 2000), a better match with tomography should result. However, this is not necessarily the case at other than the largest heterogeneity length scales (Becker & Boschi 2002). We can therefore hope that improved models with a higher degree of rheological realism (e.g. Tan *et al.* 2002) will be able to allow us to construct individual subduction zones with a higher degree of accuracy, assuming that tomography will be able to provide accurate data.

5 CONCLUSIONS

We find that the accelerating phase of subduction in the upper mantle leads to substantial slab rollback rates of the order of 0.5 of the plate speed. Once the high-viscosity lower mantle affects the slab descent, the rollback is reduced or halted for reflective boundary conditions representing flow confinement. However, for periodic boundary conditions, more appropriate for isolated subduction zones on Earth, the rollback rate remains constant in time or re-accelerates after an initial slowdown. Amongst the boundary and initial conditions considered here, a slab which is attached to a relatively immobile plate shows strongest rollback before the interaction with the 660 km boundary, since in-slab deformation is small and mass must be conserved. It is important to re-evaluate the appropriateness of 2-D models to subduction on Earth since the choice of mechanical boundary conditions turns out to be critical.

Subduction of the fixed slabs occurs due to the thinning of the lithosphere and trench retreat.

Oceanward movement of the trench is observed for most of the free and all of the fixed slabs. Only free stiff slabs are bent over backwards towards the oceanic plate at depth and penetrate straight into the lower mantle. They show continentward trench migration after the interaction with the 660 km viscosity contrast.

The subduction velocities depend on the viscosity of the slab in the initial stage and reach maximum values of the same order for reflective and periodic free slabs before the penetration of the slabs into the lower mantle.

Complexities in slab morphology such as folding are found at the ponding stage of subduction; those are enhanced by weak slabs as well as reflective boundary conditions with small aspect ratios. Both settings lead to a modulating effect of large-scale convective cells on slab morphology. For large aspect ratios and periodic boundary conditions, this folding tendency of the slab is reduced.

Only periodic boundary condition models allow the excitation of a mean horizontal motion of the lower mantle with respect to the slab that corresponds to a net relative translation of the lower mantle. For the interpretation of horizontal velocities in such models it is then important to consider the physically appropriate reference frame (Garfunkel *et al.* 1986).

ACKNOWLEDGMENTS

We would like to thank two anonymous reviewers for their constructive and helpful comments. TWB thanks Francesca Funiciello and Claudio Faccenna for discussions and was supported by the Cecil H. and Ida M. Green Foundation of IGPP, U.C. San Diego, and NSF grants EAR-0001046 and EAR-0112289. This project was funded by the Deutsche Forschungsgemeinschaft (German Research Foundation).

REFERENCES

Becker, T.W. & Boschi, L., 2002. A comparison of tomographic and geodynamic mantle models, *Geochem. Geophys. Geosyst.,* **3,** doi:2001GC000168.

Becker, T.W., Faccenna, C., O'Connell, R.J. & Giardini, D., 1999a. The development of slabs in the upper mantle: insight from numerical and laboratory experiments, *J. geophys. Res.,* **104,** 15 207–15 225.

Becker, T.W., Panasyuk, S.V., O'Connell, R.J. & Faccenna, C., 1999b. The backward-bent Indonesia slab, *EOS, Trans. Am. geophys. Un.,* **80,** S18.

Bevis, M., 1988. Seismic slip and down dip strain rate in Wadati-Benioff zones, *Science,* **240,** 1317–1319.

Bevis, M. *et al.*, 1995. Geodetic observations of very rapid convergence and backarc extension at the Tonga arc, *Nature,* **374,** 249–251.

Bock, Y., Prawirodirdjo, L., Genrich, J.F., Stevens, C.W., McGaffrey, R., Subarya, C., Puntodewo, S. S.O. & Calais, E., 2003. Crustal motion in Indonesia from Global Positioning System measurements, *J. geophys. Res.,* **108,** 2367, doi:10.1029/2001JB000324.

Byerlee, J., 1978. Friction of rock, *Pure appl. Geophys.,* **116,** 615–626.

Christensen, U.R., 1996. The influence of trench migration on slab penetration into the lower mantle, *Earth planet. Sci. Lett.,* **140,** 27–39.

Christensen, U., 2001. Geodynamic models of deep subduction, *Phys. Earth planet. Inter.,* **127,** 25–34.

Čížková, H., van Hunen, J., van den Berg, A.P. & Vlaar, N.J., 2002. The influence of rheological weakening and yield stress on the interaction of slabs with the 670-km discontinuity, *Earth planet. Sci. Lett.,* **199,** 447–457.

Conrad, C.P. & Hager, B.H., 1999. The effects of plate bending and fault strength at subduction zones on plate dynamics, *J. geophys. Res.,* **104,** 17 551–17 571.

Davies, G.F., 1995. Penetration of plates and plumes through the mantle transition zone, *Earth planet. Sci. Lett.,* **133,** 507–516.

Davies, G.F., 1999. *Dynamic Earth: Plate, Plumes and Mantle Convection,* Cambridge University Press, Cambridge.

Faccenna, C., Becker, T.W., Lucente, F.P., Jolivet, L. & Rossetti, F., 2001a. History of subduction and back-arc extension in the central Mediterranean, *Geophys. J. Int.,* **145,** 809–820.

Faccenna, C., Funiciello, F., Giardini, D. & Lucente, P., 2001b. Episodic back-arc extension during restricted mantle convection in the central Mediterranean, *Earth planet. Sci. Lett.,* **187,** 105–116.

Faccenna, C., Bellahsen, N., Funiciello, F., Jolivet, L. & Piromallo, C., 2003a. Remarks on the kinematics of the Tethyan slab, *European Geosciences Union/American Geosciences Union/European Geophysical Society, 26th General Assembly.,* Nice, 2003, Geophysical Research Abstracts, Vol. 5 (06918), SRef-ID: 1607-7962/gra/EAE03-A-06918, Copernicus GmbH, on behalf of the EGU.

Faccenna, C., Jolivet, L., Piromallo, C. & Morelli, A., 2003b. Subduction and the depth of convection in the Mediterranean mantle, *J. geophys. Res.,* **108**(B2), 2099, doi:10.1029/2001JB001690.

Fukao, Y., Widiyantoro, S. & Obayashi, M., 2001. Stagnant slabs in the upper and lower mantle transition region, *Rev. Geophys.,* **39,** 291–323.

Funiciello, F., 2002. Reconstruction of subduction processes in the Mediterranean by laboratory and numerical experiments, *PhD thesis,* Swiss Federal Institute of Technology, Zürich.

Funiciello, F., Faccenna, C., Giardini, D. & Regenauer-Lieb, K., 2003a. Dynamics of retreating slabs: 2. Insights from three-dimensional laboratory experiments, *J. geophys. Res.,* **108,** 2207, doi:10.1029/2001JB000896.

Funiciello, F., Morra, G., Regenauer-Lieb, K. & Giardini, D., 2003b. Dynamics of retreating slabs: 1. Insights from two-dimensional numerical experiments, *J. geophys. Res.,* **108,** 2206, doi:10.1029/2001JB000898.

Gaherty, J.B. & Hager, B.H., 1994. Compositional vs. thermal buoyancy and the evolution of subducted lithosphere, *Geophys. Res. Lett.,* **21,** 141–144.

Garfunkel, Z., Anderson, C.A. & Schubert, G., 1986. Mantle circulation and the lateral migration of subducted slabs, *J. geophys. Res.,* **91,** 7205–7223.

Giardini, D. & Woodhouse, J.H., 1986. Horizontal shear flow in the mantle beneath the Tonga arc, *Nature,* **319,** 551–555.

Gottschaldt, K.-D., 1997. Periodische Randbedingungen bei der zweidimensionalen numerischen Modellierung von Konvektion im Erdmantel, *Master's thesis,* Friedrich-Schiller-Universität Jena.

Gouillou-Frottier, L., Buttles, J. & Olson, P., 1995. Laboratory experiments on the structure of subducted lithosphere, *Earth planet. Sci. Lett.,* **133,** 19–34.

Griffiths, R.W., Hackney, R.I. & van der Hilst, R.D., 1995. A laboratory investigation of effects of trench migration on the descent of subducted slabs, *Earth planet. Sci. Lett.,* **133,** 1–17.

Gurnis, M. & Hager, B.H., 1988. Controls of the structure of subducted slabs, *Nature,* **335,** 317–321.

Gurnis, M., Zhong, S. & Toth, J., 2000. On the competing roles of fault reactivation and brittle failure in generating plate tectonics from mantle convection, in *The History and Dynamics of Global Plate Motions,* AGU Geophysical Monograph 121, pp. 73–94, eds Richards, M.A., Gordon, R.G. & van der Hilst, R.D., American Geophysical Union, Washington, DC.

Hager, B.H., 1984. Subducted slabs and the geoid: constraints on mantle rheology and flow, *J. geophys. Res.,* **89,** 6003–6015.

Han, L. & Gurnis, M., 1999. How valid are dynamic models of subduction and convection when plate motions are prescribed?, *Phys. Earth planet. Inter.,* **110,** 235–246.

Heidbach, O., 1999. Der Mittelmeerraum. Numerische Modellierung der Lithosphärendynamik im Vergleich mit Ergebnissen aus der Satellitengeodäsie, *PhD thesis,* Ludwig-Maximilians-Universität München.

Isacks, B. & Barazangi, M., 1977. Geometry of Benioff zones: lateral segmentations and downward bending of subducted lithosphere, in *Island arcs, Deep Sea Trenches, and Back-Arc Basins,* AGU Maurice Ewing Series 1, pp. 99–114, eds Talwani, M. & Pitman, W.C.,III, American Geophysical Union, Washington, DC.

Jarrard, R.D., 1986. Relations among subduction parameters, *Rev. Geophys.,* **24,** 217–284.

Kárason, H., 2002. Constraints on mantle convection from seismic tomography and flow modeling, *PhD thesis,* Massachusetts Institute of Technology, Cambridge, MA.

Kato, T. *et al.*, 1998. Initial results from WING, the continuous GPS network in the western Pacific area, *Geophys. Res. Lett.,* **25,** 369–372.

Kincaid, C. & Olson, P., 1987. An experimental study of subduction and slab migration, *J. geophys. Res.,* **92,** 13 832–13 840.

King, S.D. & Hager, B.H., 1990. The relationship between plate velocity and trench viscosity in Newtonian and power-law subduction calculations, *Geophys. Res. Lett.,* **17,** 2409–2412.

Letouzey, J., Werner, P. & Marty, A., 1990. Fault reactivation and structural inversion. Backarc and intraplate compressive deformations. Example of the eastern Sunda shelf (Indonesia), *Tectonophysics,* **183,** 341–362.

Lithgow-Bertelloni, C. & Richards, M.A., 1998. The dynamics of Cenozoic and Mesozoic plate motions, *Rev. Geophys.,* **36,** 27–78.

McClusky, S. *et al.*, 2000. Global Positioning System constraints on plate kinematics and dynamics in the eastern Mediterranean and Caucasus, *J. geophys. Res.,* **105,** 5695–5719.

Mitrovica, J.X. & Forte, A.M., 1997. Radial profile of mantle viscosity: results from the joint inversion of convection and postglacial rebound observables, *J. geophys. Res.,* **102,** 2751–2769.

Moresi, L. & Solomatov, V., 1998. Mantle convection with a brittle lithosphere: thoughts on the global tectonic styles of the Earth and Venus, *Geophys. J. Int.,* **133,** 669–682.

O'Connell, R.J., Gable, C.W. & Hager, B.H., 1991. Toroidal-poloidal partitioning of lithospheric plate motions, in *Glacial Isostasy, Sea-Level and Mantle Rheology,* pp. 535–551, ed. Sabadini, R., Kluwer Academic Publishers, Amsterdam.

Olbertz, D., Wortel, M. & Hansen, U., 1997. Trench migration and subduction zone geometry, *Geophys. Res. Lett.,* **24,** 221–224.

Piromallo, C. & Morelli, A., 2003. P wave tomography of the mantle under the Alpine-Mediterranean area, *J. geophys. Res.,* **108,** 2065, doi:10.1029/2002JB001757.

Ranalli, G., 1995. *Rheology of the Earth,* 2nd edn, Chapman & Hall, London.

Ricard, Y., Doglioni, C. & Sabadini, R., 1991. Differential rotation between lithosphere and mantle: a consequence of lateral mantle viscosity variations, *J. geophys. Res.,* **96,** 8407–8415.

Schmeling, H. & Marquart, G., 1991. The influence of second scale convection on the thickness of the continental lithosphere and crust, *Tectonophysics,* **189,** 281–306.

Schöffel, H.-J. & Das, S., 1999. Fine details of the Wadati-Benioff zone under Indonesia and its geodynamic implications, *J. geophys. Res.,* **104,** 13 101–13 114.

Schott, B. & Schmeling, H., 1998. Delamination and detachment of a lithospheric root, *Tectonophysics,* **296,** 225–247.

Sella, G.F., Dixon, T.H. & Mao, A., 2002. REVEL: a model for Recent plate velocities from space geodesy, *J. geophys. Res.,* **107,** 2081, doi:10.1029/2000JB000033.

Spakman, W., van der Lee, S. & van der Hilst, R., 1993. Travel-time tomography of the European-Mediterranean mantle down to 1400 km, *Phys. Earth planet. Inter.,* **79,** 3–74.

Steinberger, B., 2000. Slabs in the lower mantle—results of dynamic modelling compared with tomographic images and the geoid, *Phys. Earth planet. Inter.,* **118,** 241–257.

Steinberger, B. & O'Connell, R.J., 1998. Advection of plumes in mantle flow: implications for hotspot motion, mantle viscosity and plume distribution, *Geophys. J. Int.,* **132,** 412–434.

Tan, E., Gurnis, M. & Han, L., 2002. Slabs in the lower mantle and their modulation of plume formation, *Geochem. Geophys. Geosyst.,* **3,** doi:2001GC000238.

Tao, W.C. & O'Connell, R.J., 1993. Deformation of a weak subducted slab and variation of seismicity with depth, *Nature,* **361,** 626–628.

Tetzlaff, M. & Schmeling, H., 2000. The influence of olivine metastability on deep subduction of oceanic lithosphere, *Phys. Earth planet. Inter.,* **120,** 29–38.

Turcotte, D. & Schubert, G., 1982. *Geodynamics Application of Continuum Physics to Geological Problems,* John Wiley, New York.

van der Hilst, R.D., 1995. Complex morphology of subducted lithosphere in the mantle beneath the Tonga trench, *Nature,* **374,** 154–157.

Vassiliou, M.S. & Hager, B.H., 1988. Subduction zone earthquakes and stress in slabs, *Pure appl. Geophys.,* **128,** 547–624.

Weidner, D.J. & Wang, Y., 1998. Chemical- and Clapeyron-induced buoyancy at the 660 km discontinuity, *J. geophys. Res.,* **103,** 7431–7441.

Zhong, S., 2001. Role of ocean-continent contrast and continental keels on plate motion, net rotation of lithosphere, and the geoid, *J. geophys. Res.,* **106,** 703–712.

Zhong, S. & Gurnis, M., 1994. Controls on trench topography from dynamic models of subducted slabs, *J. geophys. Res.,* **99,** 15 683–15 695.

Zhong, S. & Gurnis, M., 1995a. Mantle convection with plates and mobile, faulted plate margins, *Science,* **267,** 838–842.

Zhong, S. & Gurnis, M., 1995b. Towards a realistic simulation of plate margins in mantle convection, *Geophys. Res. Lett.,* **22,** 981–984.